Lifetimes of Be_3^{2-} and Mg_3^{2-} Cluster Dianions

Jeremy U. Davis, Jr.,[†] Quan Manh Phung,[*,‡,¶] Takeshi Yanai,[‡,¶,§] Masahiro Ehara,[*,‖,⊥] and Thomas Sommerfeld[*,†]

†*Department of Chemistry and Physics, Southeastern Louisiana University, SLU 10878, Hammond, LA 70402, USA*

‡*Department of Chemistry, Graduate School of Science, Nagoya University, Nagoya, Aichi 464-8602, Japan*

¶*Institute of Transformative Bio-Molecules (WPI-ITbM), Nagoya University, Nagoya, Aichi 464-8602, Japan*

§*Japan Science and Technology Agency, PRESTO, Kawaguchi, Saitama 332-0012, Japan*

‖*Institute for Molecular Science and Research Center for Computational Science, Okazaki 444-8585, Japan*

⊥ *Elements Strategy Initiative for Catalysts and Batteries (ESICB), Kyoto University, Kyoto 615-8520, Japan*

E-mail: quan.phung@chem.nagoya-u.ac.jp; ehara@ims.ac.jp; Thomas.Sommerfeld@selu.edu

October 3, 2022

Abstract

The alkaline earth metal trimer cluster dianions Be_3^{2-} and Mg_3^{2-} lie energetically above their respective monoanions and can therefore decay by electron autodetachment. Consequently, these dianions possess only short-lived resonance states, and here we study these states using regularized analytic continuation as well as complex absorbing

potentials combined with a wide a variety of quantum chemistry methods including CCSD(T), SACCI, EOM-CCSD, CASPT2, and NEVPT2.

For both Be_3^{2-} and Mg_3^{2-}, four low-energy resonance states corresponding to different occupation patterns of the two excess electrons in the two lowest p-σ and p-π orbitals are identified: Two states are dominated by doubly occupied configurations and can be characterized as showing σ and π aromatic character. The other two states correspond to the open-shell singlet/triplet pair.

All dianion states are found to be highly unstable and to posses short lifetimes: They show resonance positions in the energy range of 2.3 to 4.3 eV above the ground states of their respective monoanions and broad widths between 1 and 1.5 eV translating into fs lifetimes. For both Be_3^{2-} and Mg_3^{2-}, the differences between the four states small, but the triplet states tend to be slightly more stable than the three singlet states. Thus, in the case of multi-charged ions aromatic character of the excess electrons takes second stage while Coulomb repulsion takes front and center.

In addition to the two isolated cluster dianions, model stabilization by small water clusters is explored. Our results show a dramatic drop in resonance position and width corresponding to a lifetime increase by two orders of magnitude. However, the "solvated" clusters are still resonances, and a more pronounced perturbation by, say, yet larger water clusters or a ligand environment providing larger bond dipoles, will be needed to fully stabilize two excess electrons localized on a small system such as an alkaline metal trimer.

1 Introduction

Owing to their $(ns)^2$ closed-subshell electron configuration, alkaline earth atoms occupy a middle ground between more typical metals and rare gases. The Be_2 dimer, for instance, displays typical rare gas-like behavior in that it is barely bound with respect to dissociation, yet, akin to typical metal clusters, it possesses two bound anionic states.[1,2] In contrast, the trimer behaves like a typical metal cluster: Its equilateral triangle structure (D_{3h}) is substantially more stable to dissociation than the dimer and it also possesses various anion states with binding energies of up to 1.38 eV.[2–4]

While the low-energy states of neutral Be_3 and its anion, Be_3^-, are well-established,[3] the situation is less clear for the alkaline earth trimer dianions, Be_3^{2-} and Mg_3^{2-}. In a molecular orbitals picture, the valence s orbitals of the neutral trimers are fully occupied. Consequently, the two excess electrons of the dianions must occupy orbitals arising from valence p combinations and the two lowest two are a p-σ orbital with a_1' symmetry and a p-π orbital with a_2'' symmetry. Accordingly, the following four states are possible: A closed-shell $(a_1')^2\ {}^1A_1$ state, a closed-shell $(a_2'')^2\ {}^1A_1$ state, and open-shell singlet and a triplet states corresponding to the $(a_1')^1(a_2'')^1$ occupation: ${}^1A_2''$ and ${}^3A_2''$ states (see Fig: 1 for a schematic representation).

As show in Fig: 1, two states of the dianion show ${}^1A_1$ symmetry, and it will turn out that these states are very close in energy so that we cannot distinguish them by their energetic order. We thus use Jablonski-diagram-like state labels $S_{\sigma\sigma}$, $S_{\pi\pi}$, $S_{\sigma\pi}$ and $T_{\sigma\pi}$ as indicated in Fig: 1 that indicate the dominant occupation and increase readability.

The $S_{\sigma\sigma}$ and $S_{\pi\pi}$ states have been interpreted as σ and π aromatic, and various properties of these two states and of the triplet state have been investigated for the isolated dianions[5–12] as well as for metal clusters such as $NaBe_3^-$ or Na_2Mg_3, which feature the two trimer dianions as structural units.[5,6,8] In this context, the $S_{\pi\pi}$ state can be characterized a 2π aromatic system as the bonding p-π a_2'' orbital is doubly occupied. Similarly, the $S_{\sigma\sigma}$ state can be said to possess σ-aromatic character as the bonding p-σ a_1' orbital is doubly occupied. In

Figure 1: Schematic occupation diagrams of the ground state of Be_3^- and four low-lying states of the Be_3^{2-} dianion assuming D_{3h} symmetry. For Mg_3, the inner valence consists of a $(3s)^6$ subshell, but all symmetry labels are identical.

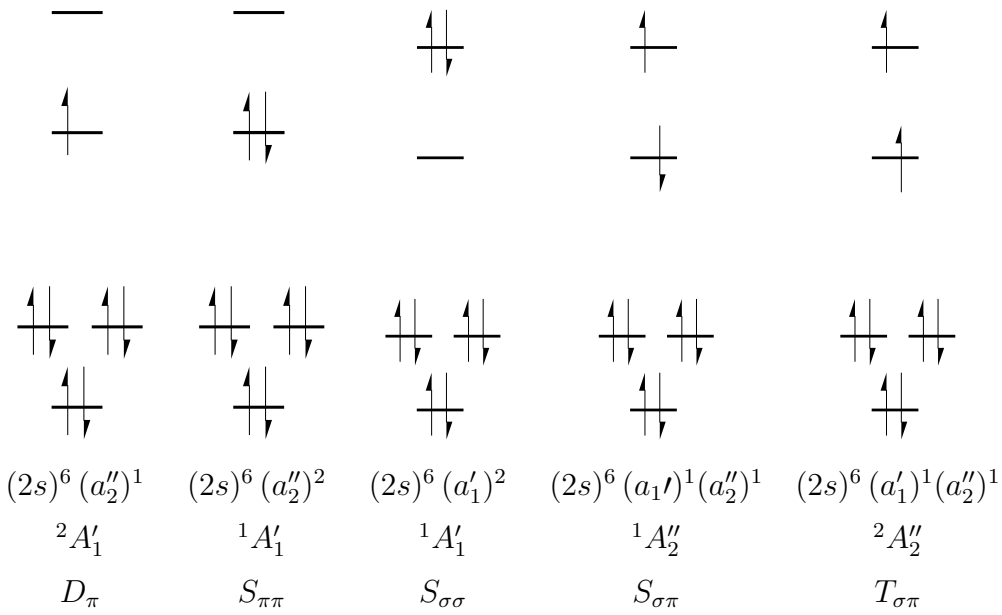

other words, in both cases the two excess electrons form a three-center, two-electron bond.[5,6]

On the other hand, one may simply consider these clusters as isolated dianions—aromatic or not—and compare their properties to the substantial established knowledge regarding small multi-charged systems.[13–15] Long-lived small dianions (less than 10 atoms or so) all follow the same building principles: A neutral or positive core surrounded by two or three subgroups with high electron affinity.[13–15] In this way, the two opposite charges can localize at the periphery of the dianion attaining maximal separation within the small molecular volume, and their substantial Coulomb repulsion can be overcome.

In contrast, the smallest known dianions with delocalized charge distributions are considerably larger (tens of atoms)[13–15] and aromatic dianions are no exception from this rule.[16] Therefore, only clusters such as $NaBe_3^-$ or Na_2Be_3 that contain Be_3^{2-} building blocks, but have net charges of zero or one, are expected to be electronically stable, while isolated Be_3^{2-} and Mg_3^{2-} dianions are expected to be metastable and to show—regardless of their aromatic character—short autodetachment lifetimes.

Let us note that the isolated-dianion perspective may explain conflicting results about the

electronic ground states and equilibrium structures of the isolated dianion (see, for example, refs. 5–12). Electronically metastable states can be understood as discreet states of an $(N+1)$-electron system that is embedded in and interacts with a continuum of states describing the N-electron system plus a free electron. In computations with finite Gaussian basis sets, this continuum is discretized and even if compact basis sets are used, the lowest state may have considerable discretized-continuum character (see e.g. discussion in section 2 of ref.[17]). Thus, if standard bound-state methods without regard to the continuum nature of the state are employed, the results will strongly depend on the electronic structure method and on the basis set because each method combination will yield a different discreet-state/discretized-continuum mixture (see for instance ref. 8).

In this paper we aim at computing energies and autodetachment lifetimes of Be_3^{2-} and Mg_3^{2-}. States metastable to autodetachment are often referred to as temporary or as resonances, and can be characterized by the energy or resonance position, E_r, of the temporary state above its decay products (here Be_3^- or Mg_3^- and a free electron with zero energy) as well as the resonance width, Γ, which is inversely related to their lifetime $\tau = \hbar/\Gamma$. These two resonance parameters are frequently combined into the complex resonance energy $E_{res} = E_r - i\Gamma/2$ because this quantity is central to many theories involving resonance.

Specifically, we study resonance positions and widths of the $S_{\sigma\sigma}$, $S_{\pi\pi}$, $S_{\sigma\pi}$ and $T_{\sigma\pi}$ states of Be_3^{2-} and Mg_3^{2-} with various quantum chemistry methods, and we discuss the influence of electron correlation on the resonance parameters in detail. Moreover, we study the complex potential energy curves of the symmetric breathing mode of the four Be_3^{2-} resonances, and we investigate how model stabilization by two water trimers and two water hexamers impacts the resonance parameters.

2 Computational Methods

Computational methods for resonances generally combine a continuum method and an electronic structure method. The continuum method is needed to address the decaying character of the resonance state, and the electronic structure method should be balanced in two ways: First, between the N and $(N+1)$-electron systems as such, and, second, within the calculation of the $(N+1)$-electron system itself: between the decaying $(N+1)$-electron character and the N-electron plus free electron character of the wavefunction. In other words, the electronic structure method must be size-extensive and internally size-extensive (c.f. introduction of ref. 18).

Currently three continuum methods are widely used: the complex absorbing potential (CAP) method,[19–22] the regularized analytical continuation (RAC) method,[23,24] and the Hazi-Taylor stabilization method.[25,26] While these three methods differ greatly in their basic ideas and underlying theory, they share the common feature of being two-step compound methods. In step 1, the electronic Hamiltonian is parameterized and *ab initio* calculations are performed for many values of the parameter. In step 2, the behavior of the computed eigenvalues as function of the parameter is analyzed to find the energy and width of the temporary state.

Each continuum method imposes somewhat different constraints on the electronic structure methods and basis sets it can be combined with. Therefore, in the following subsections, we first briefly describe the continuum methods used and then the specific electronic structure methods each was combined with.

2.1 Regularized analytic continuation calculations

This RAC method is an extrapolation method belonging to the wider family of analytic continuation of the coupling constant approaches.[23,24,27–29] In step 1 of the RAC method,

the Hamiltonian is parameterized by adding an artificial attractive potential

$$\hat{H}(\lambda) = \hat{H} + \lambda V \tag{1}$$

where the parameter λ determines the strength of the artificial attraction. For electronic resonances, the most straightforward potential is to scale the nuclear charges by $(1 + \lambda)$ because this option is readily available in many electronic structure codes. At sufficiently large values of λ the resonance becomes a bound state, and if λ is increased further, the electron binding energy will increase accordingly.

The goal is then to extrapolate the tabulated negative binding energies $E_b(\lambda)$ back to $\lambda = 0$ (we use the convention that negative binding energies correspond to bound states consistent with positive E_r values corresponding to resonances). However, naive extrapolation of the computed real energies can, at best, yield an approximation for E_r. To obtain both E_r and Γ, an extrapolation displaying the correct analytic behavior at threshold is needed.[27–29] Specifically, instead of the energy, the momentum $\kappa = \sqrt{-E(\lambda)}$ is extrapolated, extrapolation of the inverse function, $\lambda(\kappa)$, is numerically superior,[30] and consistency with various threshold laws $\kappa(\lambda)$ can be guaranteed by using tailor-made rational function approximations, so-called Padé approximants.[23]

The simplest and therefore numerically most stable Padé approximant consistent with all threshold laws is the Padé-[3,1] approximant

$$\lambda^{[3/1]}(\kappa) = \lambda_0 \frac{(\kappa^2 + 2\alpha^2\kappa + \alpha^4 + \beta^2)(1 + \delta^2\kappa)}{\alpha^4 + \beta^2 + \kappa(2\alpha^2 + \delta^2(\alpha^4 + \beta^2))}, \tag{2}$$

where λ_0, α, β, and δ are fitting parameters, and the resonance parameters are obtained from $E_r = \beta^2 - \alpha^4$ and $\Gamma = 4\alpha^2|\beta|$.[24] Here, this approximation is used for all RAC calculations.

Furthermore, in step 2 of a RAC calculation, a range of binding energies must be selected for the fitting procedure. To minimize the dependence of our results on this range, first, an approximate value of the resonance position E_r^0 was obtained from a RAC calculation with

all available data. Then the range of binding energies used in the fitting procedure was systematically extended from $-4E_r^0$ to $-7E_r^0$, and the results (typically 20 to 30 resonance energies) were averaged, using as weights the inverse of the respective χ^2 values associated with each fit. Typically, the resonance parameters depend on the data range only weakly (less than 1%) and the standard deviations are less than 20 meV.

A second consideration regarding the data range is its upper limit, that is, the inclusion of very small binding energies close to threshold. This issue has been discussed in ref. 23 (c.f. Figure 2 of ref. 23). In particular, if long-range stabilizing potentials such as scaled nuclear charges are used, at threshold, the calculation will converge on Rydberg states, which render the extrapolation unreliable. This behavior can be suppressed by using fairly compact basis sets and by discarding the first few negative binding energies. Here, we use the minimally-augmented correlation-consistent valence triple-ζ (may-cc-pVTZ)[31,32] for all RAC calculations, and we accept only binding energies more strongly bound than -0.5 eV.

From a method combination point, apart from yielding accurate electron binding energies, the RAC method places no special requirements on the electronic structure method. At an increased nuclear charge (for Be, $\lambda \approx 0.2$), the four $(N+1)$-electron states, $S_{\sigma\sigma}$, $S_{\pi\pi}$, $S_{\sigma\pi}$ and $T_{\sigma\pi}$ are stable with respect to the lowest N-electron state ($^2\mathrm{A}_2''$; D_π see Figure 1), and in principle any standard electronic structure method can be employed.

The only issue arising in the context of Be_3^{2-} and Mg_3^{2-} is static correlation, that is, the multi-configuration character of some of the involved states. Since Be and Mg possess low-lying unoccupied p-orbitals, all involved states possess a certain degree of multi-configuration character corresponding to single or double excitation into molecular orbitals deriving from these p-orbitals. If, for example, coupled-cluster with singles and doubles (CCSD)—or CCSD with perturbative triples (CCSD(T))—are performed for Be_3^- and Be_3^{2-} at $\lambda \approx 0.2$, it turns out that the D_π state is reasonably well described by CCSD—all T1 amplitudes are smaller than 0.04 and there are only two T2 amplitudes slightly larger than 0.1. Virtually the same holds true for the $S_{\pi\pi}$ state and the $T_{\sigma\pi}$ state. Thus, CCSD(T) results for these three states

should be acceptable (c.f discussion in ref. 33). In contrast, CCSD(T) cannot be used for the $S_{\sigma\sigma}$ and the $S_{\sigma\pi}$ states: The $S_{\sigma\sigma}$ state shows unacceptably large T2 amplitudes, and the $S_{\sigma\pi}$ state is an open-shell singlet.

In all coupled-cluster (and all other correlated) calculations the chemical core has been frozen. Moreover, all single-reference open-shell calculations (for the D_π and $T_{\sigma\pi}$ states) make use of the spin-unrestricted formalism as spin-contamination is minor for all open-shell states considered.

We note that similar to calculations for bound states, step 1 of a RAC/CCSD(T) calculation simultaneously provides step 1 data at the restricted or unrestricted self-consistent field (SCF) levels. The difference is, of course, that a separate step 2 analysis needs to be executed for both sets for input data. Clearly, one cannot expect SCF resonance energies to be reliable as such, however, without SCF data providing a baseline, we cannot discuss correlation effects.

Alternatives to CCSD are complete-active-space self-consistent-field (CASSCF) calculations followed by second-order perturbation theory (CASPT2) or N-electron valence perturbation theory (NEVPT2).[34] CASSCF followed by NEVPT2 is highly attractive, as it naturally describes any multi-configuration character of all relevant states in the CASSCF step, produces energies of similar quality to CASPT2, and is free of so-called intruded states. However, as for all CASSCF methods, the need to select an appropriate active space can be a distinct disadvantage.

For our RAC calculations, we chose an active space of 12 orbitals that is occupied with six, seven, and eight electrons for Be_3, Be_3^-, and Be_3^{2-} or the corresponding Mg_3 species. In other words, all valence electrons are correlated and the active space essentially corresponds to the 12 valence orbitals (2s and 2p combinations or 3s and 3p combinations, respectively).

Symmetry-adapted-cluster (SAC) configuration-interaction (SACCI) and the closely related equation-of-motion coupled-cluster (EOM-CCSD) methods represent a third alternative. Both methods need a single-configuration reference state (SAC or CCSD step), but

then energy differences with respect to the reference state can be computed for states with multi-configuration character as long as they are either one-hole states (ionization variants), one-hole-one-particle states (excitation variants), or one-particle states (attachment variants) (*c.f.*[35,36]).

In the RAC context, the $S_{\pi\pi}$ state serves as a SAC or CCSD reference state because it is bound at sufficiently large λ. Then, the electron binding energy with respect to the D_π state is computed using the ionization variants of SACCI or EOM-CCSD, while the energy difference between the $S_{\pi\pi}$ and the $S_{\sigma\pi}$ state is computed using the respective excitation variant. Using the SACCI implementation, it is also possible to compute the energy difference with respect to the $T_{\sigma\pi}$ state *via* a so-called spin-flip excitation method. Neither SACCI nor EOM-CCSD can yield reliable results for the $S_{\sigma\sigma}$ state as the $S_{\sigma\sigma}$ state differs by two excitations from the reference.

2.2 Complex absorbing potential calculations

In the complex absorbing potential (CAP) method a negative imaginary potential, $-i\eta W$ is added to electronic Hamiltonian,

$$\hat{H}(\eta) = \hat{H} - i\eta W \ , \tag{3}$$

where η is the CAP strength, and W is normally a real, positive potential that is zero at the molecule and then starts to grow with some power of the distance to the molecule.[19,37] Negative imaginary potentials absorb electron density, and a CAP absorbs the outgoing electron rending the resonance wavefunction square-integrable, provided the CAP is sufficiently strong to absorb the electron within the limitations of the basis set (finite basis sets are limited in both position and momentum space). The resonance energy is then obtained directly as a complex eigenvalue $E_{res} = E_r - i\Gamma/2$ of the complex Hamiltonian $\hat{H}(\eta)$.

In an actual CAP calculation, a trade-off must be made as η needs to be sufficiently

large to absorb the electron within the confinement of the basis set, yet too large η values cause artifacts due to reflections of the outgoing electron at the CAP boundary and by the CAP itself.[37] In other words, in CAP calculations, a sweet spot, η_{opt} must be identified. We identify this sweet spot by following the η trajectory of the resonance eigenvalue and identifying the point where the second logarithmic derivative makes a minimum.[19,37] In CAP parlance, we apply the first-order correction for CAP artifacts and identify stable points on the corrected trajectories. (Trajectories are supplied in the supporting information).

For the potential W we use a cut-off harmonic potential in the 'distance-to-the-molecule' coordinate:[38,39] In the vicinity of the nuclei W is zero, but from a cut-off radius it grows quadratically with the distance-to-the-molecule, which is defined as an average heavily biased toward the distance to the nearest atom,[38,39] making the CAP isocontours a smoothed Voronoi surface that closely follows the molecular shape similar to a van der Waals surface. Thus, the CAP displays the full, non-Abelian molecular symmetry, D_{3h}. Similar to our previous work,[18] we chose a fixed cut-off value of 3 Bohr.

The CAP is combined with the extended multi-state CASPT2 (CAP/XMS-CASPT2) method, and we followed the procedure established in our previous study.[18] Two anion states $^2\mathrm{A}_2''$ (D_π) and $^2\mathrm{A}_1'$ (D_σ) were first calculated at the CASSCF level, employing an active space identical with the RAC/CASSCF calculations, that is CAS($7e$,$12o$). We then augmented this active space with a set of n_{virt} orbitals, which are eigenfunctions of the generalized Fock operator built from the CAS($7e$,$12o$) density matrix. A projection space for the CAP calculations is then set up performing state-averaged (SA) CASCI followed by frozen-core SA-XMS-CASPT2[40–42] with an IPEA shift of 0.25 au[43] and an imaginary shift of 0.1 au,[44] and the actual CAP calculations are done in the generated subspace.[18,45]

From an electronic structure point, the main difference between the RAC and the CAP is the difference between the CAS orbitals and the CASCI step for $(N+1)$ electron states. Moreover, the one-particle basis set used in the RAC calculations is far more compact. In contrast to these differences, the difference between NEVPT2 and CASPT2 is minor.

Owing to various bottlenecks in our current CAP/XMS-CASPT2 code, we were forced to limit n_{virt} severely: For the $S_{\pi\pi}$, $S_{\sigma\pi}$, and $T_{\sigma\pi}$ states, we selected five a_2'' virtual orbitals leading to CAS(8e,17o) active spaces, and for the $S_{\sigma\sigma}$ state, we selected four a_1' virtual orbitals generating a CAS(8e,16o) active space. The respective virtual orbitals were chosen based on their symmetry and on their energy giving preference to virtual orbitals closer to the expected resonance position as inferred from compact basis set XMS-CASPT2 calculations for the state in question.[17] In practice, this procedure translates into projection states lying between 2 and 5 eV above the two anion states (see also Figures S1-S4). We note that a larger number of averaged anion states and active orbitals would be desirable (see discussion in section 3), however, the computational cost grows too rapidly with n_{virt} for our resources.

For the CAP calculations the may-cc-pVTZ set was augmented with a second diffuse s function (exponent 0.00735), its diffuse p exponent was replaced with 0.014, and four additional diffuse p functions were added using an even-scaling factor of 1.6, that is, the smallest p exponent is 0.002136.

Four quantum chemistry packages were used. SAC-CI calculations were performed with a developers' version of GAUSSIAN09, Revision B.01.[46] Version 2.1 of the CFOUR package[47] was used for CCSD(T) and EOM-CCSD calculations. XMS-CASPT2 calculations were performed with the orz program package.[48] ORCA version 4.2.1[49] was used for the NEVPT2 calculations. Moreover, the pair-natural-orbital EOM-CCSD (PNO-EOM-CCSD) implementation available in ORCA[50] was used to study the solvated trimer dianions.

3 Results and Discussion

The goal of this paper is to explore energies and autodetachment lifetimes of Be_3^{2-} and Mg_3^{2-}. Based on the general behavior of small dianions as well as on the inability of Be or Mg atoms to bind excess electrons, we do not expect to find any regions in nuclear coordinate space where either of these dianions can bind both excess electrons. The relevant questions are

then: "How unstable are the dianions with respect to the monoanion?" and "How long do the dianions typically live?". We focus primarily on D_{3h} symmetrical structures at geometries between the neutral and the anion as the lowest electronic states of both neutral Be_3 and Be_3^- are trigonal planar and the same is true for the corresponding Mg species. Moreover, we investigate the symmetric breathing mode of Be_3, Be_3^-, and Be_3^{2-} over a range that covers some of the structures discussed in ref. 6–11,51.

3.1 Be_3^{2-} resonance states

We begin with a comparison of results obtained at a fixed D_{3h} geometry with $R = 2.15\,\text{Å}$, a bond length between the minimal bond lengths of Be_3 and the Be_3^-.[3] First, we compare different electronic structure methods keeping the continuum method fixed, then we compare our RAC and CAP results.

Combing the RAC with various electronic structure methods yields the resonance parameters listed in Table 1. These positions and widths vary substantially. Even if only the correlated methods CCSD(T), SACCI, and NEVPT2 are considered, variations are still in the order of half an eV, which is not entirely unexpected as the system combines two challenges: On the one hand, computing electron binding energies represents a challenge as such, and even for "easy" systems, deviations of several tenths of an eV between binding energies from different electronic structure methods are common. On the other hand, despite most states possessing one dominating configuration, static correlation effects are present, but different for each state. Since none of the employed electronic structure methods is perfect, but rather possesses its own unique strengths and weaknesses regarding these two challenges, good agreement between methods as different as CCSD(T), SACCI, and NEVPT2 may be considered at worst suspicious, at best fortuitous.

Trends between different methods can be studied for the $S_{\pi\pi}$ and the $T_{\sigma\pi}$ state, as energies of these two states can be obtained with uncorrelated SCF, partially correlated CASSCF, and all three correlated methods, NEVPT2, CCSD(T), and SACCI. The correlated

Table 1: RAC resonance energies of the four Be_3^{2-} states for D_{3h} symmetry and $R = 2.15\,\text{Å}$. E_r is measured relative to the D_π state of Be_3^- computed with the same method at the same geometry.

		E_r [eV]	Γ [eV]
$S_{\sigma\sigma}$	NEVPT2	3.68	2.12
$S_{\pi\pi}$	SCF	4.16	2.05
	CASSCF	4.21	1.92
	NEVPT2	3.41	1.77
	CCSD(T)	3.12	1.42
	SACCI	2.90	1.56
$S_{\sigma\pi}$	NEVPT2	3.51	1.75
	SACCI	2.89	1.63
$T_{\sigma\pi}$	SCF	2.58	1.06
	CASSCF	3.90	1.90
	NEVPT2	3.21	1.56
	CCSD(T)	2.83	1.39
	SACCI	2.51	1.44

methods agree reasonably well with each other (variations in the order of 0.5 eV) and for both states, NEVPT2 predicts the highest resonance position, SACCI predicts the lowest, and CCSD(T) is fairly close to the mean of the other two correlated methods. The widths follow a slightly different order, with NEVPT2 predicting the largest widths, CCSD(T) predicting the smallest, and SACCI predicting widths slightly larger than CCSD(T).

In particular, the CCSD(T)–NEVPT2 trend can be compared to the predicted electron affinities (EA) of these two methods that can be inferred from the potential energy curves discussed below. According to the high-level multi-reference configuration interaction results from ref. 3, the $^1A_1'$ (S_0) ground state of the Be_3 has a minimal-energy bond length of 2.203 Å, the D_π ground state of the anion has a minimal-energy bond length of 2.106 Å, and the energy difference between these two structures, the EA, is −1.38 eV. The NEVPT2 bond lengths compare well with these reference values, but the NEVPT2 value of −1.22 eV underestimates the EA. In contrast, the CCSD(T) bond lengths are a bit too long (see below), but the CCSD(T) EA of −1.35 eV is very close to ref. 3.

As NEVPT2 underestimates the binding energy of the first electron, one may expect that it would do the same for the second excess electron, which would translate into a too high E_r. In contrast, CCSD(T) predicts the first electron binding energy quite reliably, and one may therefore expect that it also predicts the second with similar reliability adding weight to the trend-derived argument that CCSD(T) probably yields the most reliable resonance positions.

These arguments are, of course, anything but watertight, and either experimental or significantly more costly computational results from, say, diffusion Monte-Carlo approaches, are needed to draw final conclusions. Still, the observed trends suggest that all three correlated methods predict semi-qualitative resonance energies at the very least, if not better.

While SCF and CASSCF are generally unreliable for predicting electron binding energies,[52] and there is no reason to expect that their RAC combinations will predict useful resonance parameters, they provide the basis to study electron correlation in resonances. For the $S_{\pi\pi}$ state, SCF and CASSCF agree closely, and both methods predict significantly higher resonance positions as well as higher widths than the correlated methods. In other words, the $S_{\pi\pi}$ state shows as much static correlation as the D_π state, and dynamic electron correlation stabilizes the $S_{\pi\pi}$ state as one would expect based on a simple number-of-electrons argument.

Yet, for the $T_{\sigma\pi}$ state, SCF and CASSCF differ significantly, with SCF predicting the smallest width of all methods and a position as low as SACCI whereas CASSCF predicts the highest position and width. While the $T_{\sigma\pi}$ state apparently shows far less static correlation than the D_π state, dynamic electron correlation again stabilizes the $(N+1)$-electron system. Thus, a single-reference wavefunction definitely has the potential to muddy the water, but after CASSCF levels the playing field, dynamic correlation always stabilizes the resonance.

Having discussed the effect of electron correlation, we now briefly compare RAC (Table 1) with CAP (Table 2) calculations. Due to the close relationship between CASPT2 and NEVPT2, one may expect CAP/CASPT2 and RAC/NEVPT2 to agree rather well, and this

Table 2: CAP/XMS-CASPT2 resonance energies of the four Be_3^{2-} states for D_{3h} symmetry and $R = 2.15$ Å. E_r is measured relative to the D_π state of Be_3^- at the same geometry.

	E_r [eV]	Γ [eV]
$S_{\sigma\sigma}$	3.64	0.52
$S_{\pi\pi}$	3.87	0.49
$S_{\sigma\pi}$	3.75[a]	0.47[a]
$T_{\sigma\pi}$	3.40[a]	0.41[a]

[a]Only uncorrected results available.

is indeed true for the resonance positions. However, CAP/CASPT2 predicts significantly smaller widths than RAC/NEVPT2.

The small widths in our current CAP calculations is in all likelihood unrelated to the CAP method as such but rather to the projection space employed for setting up the CAP Hamiltonian (subsection 2.2). In this context, a resonance is best understood as a discrete state with energy E_d that is embedded in and interacts with a continuum of states, so that it acquires a width Γ (Weisskopf-Fano-Feshbach picture). Thus, Γ characterizes not only the resonance lifetime, but also the energy range over which the discrete state interacts with the continuum.

In a finite basis set context, the continuum is replaced with a discrete representation of so-called discretized continuum states, and Γ provides a rough measure of the energy range of states that are needed to describe the resonance wavefunction in a projection formalism.[45] Owing to various bottlenecks in our current CAP/XMS-CASPT2 code, we were forced to use a roughly 3 eV energy window to set up the CAP projection spaces (see subsection 2.2). While this range comfortably exceeds the resonance widths predicted by the RAC method by at least a factor of two, the discrete state-continuum interaction is characterized by a Breit-Wigner distribution, and its tails are expected to contribute significantly. Indeed, all our subspace vectors contribute appreciably to the resonance at the optimal CAP strength, while a fully converged subspace is indicated by vanishing contributions at the low and high energy tails. Therefore, the CAP/CASPT2 calculations are able to reproduce reliable

resonance positions in very good agreement with RAC/NEVPT2, but the CAP widths are not fully converged and underestimate the true width.

Regardless of method variations, all four dianion states are predicted to represent short-lived resonance states with energies in the range of 2.5 to 3.5 eV above the ground state of Be_3^- and lifetimes in the order of 1 fs or less. Thus, as isolated entities, all four Be_3^{2-} states are—as expected—exceedingly short-lived, and we predict that these dianion states can only be observed as Be_3^{2-} building blocks in a stabilizing environment (see section 1 and 3.4) or, possibly, as broad resonances in electron scattering from stable states of Be_3^-.

3.2 Mg_3^{2-} resonance states

The corresponding four Mg_3^{2-} resonance states have been studied at a fixed Mg–Mg distance of 3.38 Å close to the equilibrium geometry of the $S_{\pi\pi}$ state,[6] and our results are collected in Table 3.

The Mg_3^{2-} results follow very similar trends as the Be_3^{2-} data: While the fully correlated NEVPT2, CCSD(T), and EOM-CCSD (replacing the closely related SACCI, which we used for Be_3^{2-}) methods agree reasonably well, SCF and CASSCF results deviate from the predictions of the former. Focusing on the three correlated methods only, similar to Be_3^{2-}, NEVPT2 tends to predict the highest resonance position, while EOM-CCSD predicts the lowest positions, and the CCSD(T) positions lie between the two.

Based on the comparison with the ^2P_u resonance states of the atomic anions Be^- and Mg^-,[53] one may expect the Mg_3^{2-} resonances to be more stable than the corresponding Be_3^{2-} states. This expectation holds true for the $S_{\pi\pi}$, the $S_{\sigma\pi}$, and $T_{\sigma\pi}$ states, but is incorrect for the $S_{\sigma\sigma}$ state. While there are some slight variations between methods and states, it is fair to say that in going from Be_3^{2-} to Mg_3^{2-}, the former three states are stabilized by roughly 0.6 eV. Their widths also decrease by several tenths of an eV, however, the trend for the widths is less uniform. In contrast, the $S_{\sigma\sigma}$ of Mg_3^{2-} is predicted to lie energetically slightly higher than the $S_{\sigma\sigma}$ in Be_3^{2-}, yet, at the same time, it is predicted to show a substantially

Table 3: RAC resonance energies of the four Mg_3^{2-} states for D_{3h} symmetry and $R = 3.38$ Å. E_r is measured relative to the D_π state of Mg_3^- computed with the same method at the same geometry.

		E_r [eV]	Γ [eV]
$S_{\sigma\sigma}$	NEVPT2	3.83	1.69
$S_{\pi\pi}$	SCF	3.28	1.40
	CASSCF	3.44	1.72
	NEVPT2	2.92	1.69
	EOM-CCSD	2.45	1.06
	CCSD(T)	2.59	1.02
$S_{\sigma\pi}$	NEVPT2	2.81	1.17
	EOM-CCSD	2.32	1.19
$T_{\sigma\pi}$	SCF	2.74	1.22
	CASSCF	3.24	1.31
	NEVPT2	2.62	1.05
	CCSD(T)	2.30	1.02

smaller width indicating a "stabilization" in a lifetime sense.

3.3 Potential energy curves

For the $^1A_1'$ ground state of Be_3 (S_0 state) and the D_π state of Be_3^-, potential energy curves (PEC) along the totally symmetric breathing modes (D_{3h} symmetry is maintained while the Be–Be bond length R is changed) can be computed in a straightforward manner. PECs for the four dianionic states $S_{\sigma\sigma}$, $S_{\pi\pi}$, $S_{\sigma\pi}$, and $T_{\sigma\pi}$ can then be obtained by adding the respective resonance positions to the D_π PEC. However, these four PECs should be taken with a grain of salt as their widths are large and the three singlet states will be coupled by D_{3h} symmetry-breaking vibrations.[54] Nonetheless, the PECs provide a useful quantitative representation for discussing electron loss processes and relative stabilities.

PECs obtained with CCSD(T) are shown in the left panel of Figure 2. In comparison with the reliable MRCI results from ref. 3, CCSD(T) predicts somewhat longer bond lengths for Be_3 and Be_3^- presumably due to a combination of missing static correlation effects and the small triple-ζ basis used here. The trend, however, agrees very well: The Be–Be bond

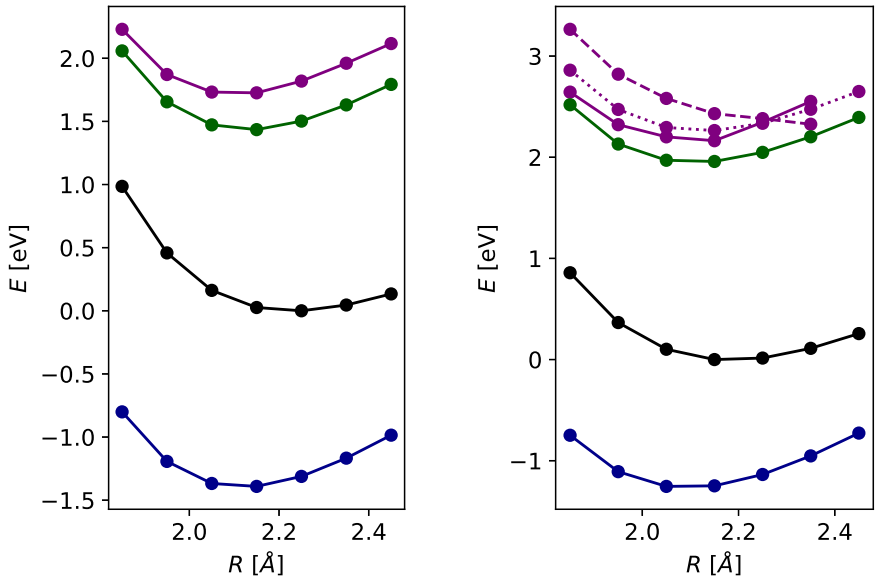

Figure 2: D_{3h} potential energy curves for Be_3 (black), Be_3^- (blue), and Be_3^{2-}. The left and right panels show CCSD(T) and NEVPT2 results, and R is the Be–Be distance. Color scheme: black: Be_3 S_0, blue: Be_3^- D_π, green: Be_3^{2-} $T_{\sigma\pi}$, purple: all Be_3^{2-} singlet states (solid: $S_{\pi\pi}$, dashed: $S_{\sigma\sigma}$, dotted: $S_{\sigma\pi}$).

length in the anion is about 0.1 Å shorter than in the neutral. Moreover, as discussed above, the predicted EA (1.35 eV) agrees well with the value of 1.38 eV from ref. 3.

As the resonance positions of both the $S_{\pi\pi}$ and $T_{\sigma\pi}$ states changes only slightly (about 0.1 eV over the bond length range shown), the dianion PECs follow the D_π curve closely, and the "minimal energy structures"—to the extent that one can define a minimal energy structure of a resonance—is correspondingly close to the structure of the D_π ground state of the anion.

The corresponding NEVPT2 PECs are shown in the right panel of Figure 2. As discussed above, the bond lengths predicted at this computational level—2.22 Å for the S_0 and 2.13 Å for the D_π state—are much closer to the high quality results from ref. 3. However, the NEVPT2 EA is 0.16 eV too low (see above) suggesting that the dianion PECs are slightly too high.

Similar to CCSD(T), the PECs of the dianionic resonance states follow the D_π curve closely as the four resonance positions change only very little over the bond length range

shown: The $S_{\sigma\sigma}$ position changes by roughly 0.6 eV, the other three positions by less than 0.2 eV. More importantly, all four resonance positions change in an almost linear fashion with the Be–Be distance and therefore the minima on the dianion PECs are only slightly shifted with respect to the D_π minimum.

Our complex PECs directly contradict the real-valued PEC from ref. 51 that suggest the presence of two D_{3h} symmetrical minima with bond-lengths close to 2.078 Å and 2.156 Å. We cannot directly comment on these density functional results, but it seems likely that the two identified minima can be understood in the Weisskopf-Fano-Feshbach picture (see section 2): One may assume that one minimum corresponds to a state showing essentially discrete state character, while the other minimum corresponds to a state showing essentially discretized-continuum state character. In other words, one minimum corresponds to Be_3^{2-}, while the other minimum corresponds to Be_3^- and a "free" electron confined by the basis set. To avoid unwanted discretized-continuum minima, approaches such as RAC, CAP, or the stabilization method are needed.

3.4 Model stabilization

Having found the isolated dianions Be_3^{2-} and Mg_3^{2-} to possess only short-lived resonance states well above the ground states of the respective monoanions, in this section we consider a Be_3^{2-} dianion embedded in a stabilizing environment. Specifically, we investigate the resonance position and lifetime of the $S_{\pi\pi}$ states as its closed-shell single-reference character enables us to optimize the stabilizing environment for the respective dianion with second-order many-body perturbation theory (MP2). Such an optimization of a resonance with standard methods is possible as the environment-stabilized dianions are much lower in energy than their isolated counterparts and as the sought state lies well below all discretized continuum states as long as normal basis sets with standard diffuse functions are used.[17]

As mentioned in the introduction, stabilization of Be_3^{2-} and Mg_3^{2-} by cations and point charges has been considered previously.[5,6,8] The impact of a full positive charge is, of course,

drastic, and it is hardly surprising that, for example, the highest occupied orbital of Mg_3Na^- shows a large contribution from the Na valence orbitals.[5] Instead of a cation stabilizing a dianion, it seems therefore more appropriate to think of anions such as $NaBe_3^-$ and $NaMg_3^-$ as metal clusters with two excess electrons in their "conduction bands". The two excess electrons are distributed throughout the metal cluster, and owing to the single negative net charge, the cluster anion as such is stable to electron loss.

In contrast, a stabilizing environment would not participate directly in the bonding of the excess electrons, but rather serve in an auxiliary role, say, an explicit interaction with solvent molecules or a more implicit one with a polarizable continuum. Of course, distinguishing direct from indirect participation is anything but straightforward, and where and whether to draw a clear-cut dividing line is a matter of taste. A reasonable distinction may be the nature of the bound state of the frozen environment without Be_3^{2-} or Mg_3^{2-} being present: If the environment can bind an excess electron in a valence state, it can actively participate in the stabilization as a mixing of dianion and environment valence will occur in the combined system. If, on the other hand, the environment supports only non-valence states (surface-bound, cavity-bound, etc.), its role can be characterized as supporting as valence mixing can be neglected.

Here, we consider a weaker stabilization in the form of two water clusters that point dangling hydrogen bonds at both lobes of the π-system (see Figure 3). Water clusters are employed as their electrostatic interactions are well-understood, clusters with increasing total dipole moments are easily constructed, and a well-defined structure is guaranteed by the internal hydrogen bonds in each cluster.

Specifically, two Be_3^{2-}–water and one Mg_3^{2-}–water clusters are considered: $Be_3((H_2O)_3)_2^{2-}$, $Mg_3((H_2O)_3)_2^{2-}$, and $Be_3((H_2O)_6)_2^{2-}$ (Figure 3). For the former two clusters, the stabilizing environment is provided by two water trimers; for the latter, the stabilizing environment is provided by two water hexamers.

We emphasize that these clusters are by no means intended to represent realistic micro-

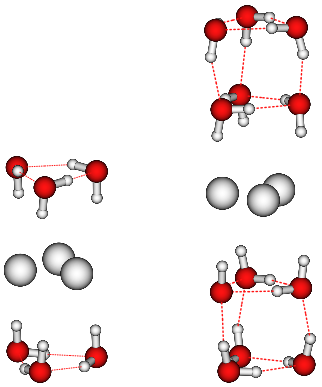

Figure 3: Structures of the $Be_3((H_2O)_3)_2^{2-}$ and $Be_3((H_2O)_6)_2^{2-}$ clusters considered as model solvation environments. Both clusters display D_3 symmetry. $Mg_3((H_2O)_3)_2^{2-}$ looks almost exactly as $Be_3((H_2O)_3)_2^{2-}$.

solvation or an actual solvation model, but rather a model stabilization of water clusters with "solvating" hydrogen bonds arranged so as to deliberately point at the π-system. In aqueous solution, it is highly likely that any alkaline earth metal cluster—regardless of its charge—will react with water to form solvated atomic dications and reaction products suitable for the total charge of the original cluster (H_2 and OH^- for neutral clusters). In addition, in water the dianions may autodetach into cavity or surface states. We suppress this pathway in our calculations by the choice of a rather compact basis set and a structure that fails to support cavity or surface states once the metal cluster is present.

While our specific clusters should be understood as model systems, let us emphasize that it may be possible to observe the decay of Be_3^{2-} or Mg_3^{2-} in very cold, ice-like water clusters in the gas phase. For such a system, it is conceivable to detect the resonance as an excited state of a cluster dianion whose ground state consists of a Be_3^- unit embedded in a water cluster that also supports a surface or cavity state. Similar scenarios are imaginable in solution, provided the Be_3^- unit is protected by a polydentate ligand. Then a solvated electron can be excited into a temporary Be_3^{2-} state.

All three clusters considered here, on the other hand, have deliberately been constructed to serve only in a stabilizing and no other role. All three represent local minima in compact basis set (MP2/ma-def2-TZVP(-f)[55,56]) model chemistries,[17] and all three show essentially

D_3 symmetry. Note that the solvating hydrogen bonds point between two metal atoms creating an "interlocked" structure. The Cartesian coordinates of these structures are available in the supporting information.

Table 4: RAC/PNO-EOM-CCSD resonance energies of $S_{\pi\pi}$ states of Be_3^{2-} and Mg_3^{2-} in a model solvation environment.

	E_r [eV]	Γ [eV]
Be_3^{2-}	2.90	1.51
$Be_3((H_2O)_3)_2^{2-}$	1.49	0.102
$Be_3((H_2O)_6)_2^{2-}$	0.525	0.0109
Mg_3^{2-}	2.35	1.07
$Mg_3^{2-}((H_2O)_3)_2^{2-}$	1.55	0.229

Resonance positions and widths for the $S_{\pi\pi}$ states of the isolated and solvated trimers are collected in Tab. 4. Solvation stabilizes the trimer dianions substantially: For example, in the Be_3^{2-}, $Be_3((H_2O)_3)_2^{2-}$, $Be_3((H_2O)_6)_2^{2-}$ series, the resonance position drops from about 3 to 1.5 and 0,5 eV, and the width decreases (the lifetime increases) by roughly an order of magnitude in going to a water trimer and yet another order of magnitude by going to water hexamer environment. Nonetheless, all dianions investigated are still resonance states with finite lifetimes.

In comparison with clusters such as Be_3Na_2 and Be_3Na^-, solvating water molecules represent a much weaker perturbation of the Be_3^{2-} core than the metal cation environment, as the water cluster model environment stabilizes the excess electrons by hydrogen bonding, essentially a dipole effect. In their frozen geometries, the solvating water trimers and hexamers support only dipole-bound anion states (in its equilibrium geometry, the water trimer does not support any anion state), and the frozen non-polar $((H_2O)_3)_2$ and $((H_2O)_6)_2$ scaffolds support non-valence bound states with binding energies of about 0.6 and 1.6 eV (PNO-EOM-CCSD; aug-cc-pVDZ basis augmented with a (7s7p4d) set at the symmetry center between the trimers or hexamers respectively–much lower than the electron affinity of a Na^+ ion (5.14 eV).

The difference in electron binding energy of the stabilizing units is directly reflected in the electron binding energies of the corresponding Be_3^{2-} clusters: Na^+ is a cation with a massive electron affinity, Be_3Na^- processes only a single negative charge, and the Be_3Na^- anion is stable to electron loss. In contrast, both $Be_3((H_2O)_3)_2^{2-}$ and $Be_3((H_2O)_6)_2^{2-}$ are doubly charged anions, and both are still resonance states unstable to electron loss yet in comparison with isolated Be_3^{2-} their lifetimes are substantially longer.

4 Summary and Conclusions

We have studied resonance states of the isolated and "solvated" dianions Be_3^{2-} and Mg_3^{2-}. Electronic resonances are unstable with respect to electron autodetachment, and the dianion states considered here are unstable with respect to decay into one of several monoanion states and a free electron as well as to decay into the neutral and two free electrons. However, we expect the latter process to be considerably slower than the former as the former is a straightforward one-electron decay, whereas the latter involves a synchronous two-electron process and has a much higher threshold.

All quantum chemistry methods for resonance states consist of a combination of a continuum method with an electronic structure method. Most of our calculations employed the RAC continuum approach, and unfortunately we were unable to compare the RAC method fairly with the CAP approach as we were forced to make compromises setting up the projection subspace for our CAP calculation, which probably impacted the CAP widths. Moreover, we were unable to compare with stabilization calculations, which are non-trivial for the same reasons that render setting up a CAP subspace challenging: The lack of a closed-shell reference or parent state, a high density of states, and large widths. On the other hand, we were able to compare multiple electronic structure methods and investigate electronic correlation effects in detail.

Four low-lying states have been identified that correspond to different occupation patterns

of the two excess electrons in the lowest p-σ and p-π orbitals. For the isolated dianions, all four states show resonance positions in the range of 2 – 4 eV above the ground states of the respective monoanions and broad decay widths in the 1 – 1.5 eV range. In other words, all four dianion states—regardless of any aromatic character—represent short-lived unstable species. In fact, our calculations predict the triplet $T_{\sigma\pi}$ state to be the most "stable" dianion in the sense that it possesses the smallest resonance position and smallest width for both Be_3^{2-} and Mg_3^{2-}. Thus, regarding the stability of excess electrons of multi-charged negative ions, Coulomb repulsion plays the leading role, while aromatic character plays only a supporting part.

Potential energy curves along the D_{3h} symmetry conserving breathing mode were studied for Be_3^{2-}. It turns out that the resonance position of the four dianions changes only slowly and almost linearly with the Be–Be bond length. Therefore, the four dianion PECs essentially follow the D_π state of Be_3^-. However, the four states are much broader than their respective energy differences, and symmetry-breaking vibrations will couple the three singlet states.

Having identified all low-energy states of Be_3^{2-} and Mg_3^{2-} as short-lived resonances, we investigated the influence of a stabilizing environment on the $S_{\pi\pi}$ state. Adding two water trimers above and below the Be_3^{2-} and Mg_3^{2-} planes respectively, where each water cluster points three dangling hydrogen-bond towards a metal-metal bond, leads to a reduction of the resonance positions to about 1.5 eV and a substantial increase in lifetime (by factors of 15 and 5 for Be_3^{2-} and Mg_3^{2-}). Replacing the water trimers with water hexamers almost stabilizes Be_3^{2-}: Its position is as low as 0.5 eV and its width is a mere 10 meV. Our studies thus show that—as one may expect—a strongly perturbing environment is needed to stabilize two excess electrons on a small cluster without electron-affine substructures.

5 Supporting Information

Included: η-trajectories associated with the CAP calculations; Cartesian coordinates of $Be_3((H_2O)_3)_2^{2-}$, $Be_3((H_2O)_6)_2^{2-}$, and $Mg_3((H_2O)_3)_2^{2-}$.

Acknowledgments

T.S. gratefully acknowledges support from the National Science Foundation under Grant No. 1856775. T.Y. is supported by JST, PRESTO Grant Number 17937609. M.E. is supported by JSPS (Grant numbers JP16H06511, JP20H02718).

References

(1) Meshkov, V. V.; Stolyarov, A.; Heaven, M. C.; Haugen, C.; LeRoy, R. J. Direct–potential–fit analyses yield improved empirical potentials for the ground $X^1\Sigma_g^+$ state of Be_2. *J. Chem. Phys.* **2014**, *140*, 064315.

(2) Kalemos, A. The nature of the chemical bond in Be^{2+}, Be_2, Be_2^-, and Be_3. *J. Chem. Phys.* **2016**, *145*, 214302.

(3) Kalemos, A. Be_3^-, an ab initio study. *Chem. Phys. Lett.* **2020**, *739*, 136964.

(4) Diaz-Torrejonand F. Espinosa-Magana, C. C.; Kaplan, I. G. Comparative theoretical study of the electron affinities of the alkaline-earth clusters: Be_n, Mg_n, and Ca_n ($n = 2, 3$). *Int. J. Quant. Chem.* **2011**, *111*, 103–110.

(5) Kuznetsov, A. E.; Boldyrev, A. I. A single π-bond captures 3, 4 and 5 atoms. *Chem. Phys. Lett.* **2004**, *388*, 452–456.

(6) Oscar, J.; Jiménez-Halla, C.; Matito, E.; Blancafort, L.; Robles, J.; Solà, M. Tuning

aromaticity in trigonal alkaline earth metal clusters and their alkali metal salts. *J. Comput. Chem.* **2009**, *30*, 2764–2776.

(7) Giri, S.; Roy, D. R.; Duley, S.; Chakraborty, A.; Parthasarathi, R.; Elango, M.; Vijayaraj, R.; Subramanian, V.; Islas, R.; Merino, G.; Chattaraj, P. K. Bonding, aromaticity, and structure of trigonal dianion metal clusters. *J. Comput. Chem.* **2010**, *31*, 1815–1821.

(8) Oscar, J.; Jiménez-Halla, C.; Matito, E.; Blancafort, L.; Robles, J.; Solà, M. Tuning aromaticity in trigonal alkaline earth metal clusters and their alkali metal salts. [Erratum to document cited in CA152:021072. *J. Comput. Chem.* **2011**, *32*, 372–373.

(9) Brito, B. G. A.; Hai, G.; Candido, L. Correlation effects on aromaticity of Be_3^{2-} cluster: A quantum Monte Carlo study. *Chem. Phys. Lett.* **2013**, *568*, 108–110.

(10) Mondal, S.; Chattaraj, P. K. Stability and structural dynamics of Be_3^{2-} clusters. *Chem. Phys. Lett.* **2014**, *593*, 128–131.

(11) Goswami, T.; Paul, S.; Mandal, S.; Misra, A.; Anoop, A.; Chattaraj, P. K. Unique bonding pattern and resulting bond stretch isomerism in Be_3^{2-}. *Int. J. Quant. Chem.* **2015**, *115*, 426–433.

(12) Pan, S.; Jana, G.; Saha, R.; Zhao, L.; Chattaraj, P. K. Intriguing structural, bonding and reactivity features in some beryllium containing complexes. *Phys. Chem. Chem. Phys.* **2020**, *22*, 27476–27495.

(13) Scheller, M. K.; Compton, R. N.; Cederbaum, L. S. Gas-phase multiply charged anions. *Science* **1995**, *270*, 1160.

(14) Dreuw, A.; Cederbaum, L. S. Multiply charged anions in the gas phase. *Chem. Rev.* **2002**, *102*, 181.

(15) Simons, J. Molecular anions. *J. Phys. Chem. A* **2008**, *112*, 6401.

(16) Sommerfeld, T. A fresh look at aromatic dianions. *J. Am. Chem. Soc.* **2002**, *124*, 1119.

(17) Sommerfeld, T.; Weber, R. J. Empirical Correlation Methods for Temporary Anions. *J. Phys. Chem. A* **2011**, *115*, 6675–6682.

(18) Phung, Q. M.; Komori, Y.; Yanai, T.; Sommerfeld, T.; Ehara, M. Combination of a Voronoi-type complex absorbing potential with the XMS-CASPT2 method and pilot applications. *J. Chem. Theory Comput.* **2020**, *16*, 2606–2616.

(19) Santra, R.; Cederbaum, L. S. Non-Hermitian electronic theory and application to clusters. *Phys. Rep.* **2002**, *368*, 1–117.

(20) Sajeev, Y.; Ghosh, A.; Vaval, N.; Pal, S. Coupled-cluster methods for autoionization resonances. *Int. Rev. Phys. Chem.* **2014**, *33*, 397 – 425.

(21) Jagau, T.-C.; Bravaya, K. B.; Krylov, A. I. Extending Quantum Chemistry of Bound States to Electronic Resonances. *Annu. Rev. Phys. Chem.* **2017**, *68*, 525–553.

(22) Basumallick, S.; Sajeev, Y.; Pal, S.; Vaval, N. Negative ion resonance states: The Fock-space coupled-cluster way. *J. Phys. Chem. A* **2020**, *124*, 10407–10421.

(23) Horáček, J.; Paidarová, I.; Čurík, R. On a simple way to calculate electronic resonances for polyatomic molecules. *J. Chem. Phys.* **2015**, *143*, 184102:1–7.

(24) Čurík, R.; Paidarová, I.; Horáček, J. The 2Πg shape resonance of acetylene anion: an investigation with the RAC method. *Eur. Phys. J. D* **2016**, *70*, 146.

(25) Falcetta, M. F.; DiFalco, L. A.; Ackerman, D. S.; Barlow, J. C.; Jordan, K. D. Assessment of various electronic structure methods for characterizing temporary anion states: Application to the ground state anions of N_2 , C_2H_2, C_2H_4, and C_6H_6. *J. Phys. Chem. A* **2014**, *118*, 7489 –7497.

(26) Thodika, M.; Fennimore, M.; Karsili, T. N. V.; Matsika, S. Comparative study of methodologies for calculating metastable states of small to medium-sized molecules. *J. Chem. Phys.* **2019**, *151*, 244104.

(27) Kukulin, V. I.; Krasnopolsky, V. M. Description of few-body systems via ACCC. *J. Phys. A* **1977**, *10*, L33.

(28) Krasnopolsky, V. M.; Kukulin, V. I. Theory of resonance states based on ACCC. *Physics Letters* **1978**, *69A*, 251.

(29) Kukulin, V. I.; Krasnopolsky, V. M.; Horáček, J. *Theory of Resonances*; Kluwer Acedmic Publishers, Dordrecht, The Netherlands, 1989.

(30) Horáček, J.; Paidarová, I.; Čurík, R. Determination of the Resonance Energy and Width of the $^2B_{2g}$ Shape Resonance of Ethylene with the Method of Analytic Continuation of the Coupling Constant. *J. Phys. Chem. A* **2014**, *118*, 6536–6541.

(31) Prascher, B. P.; Woon, D. E.; David, E.; Peterson, K. A.; Dunning, T. H.; Wilson, A. K. Gaussian basis sets for use in correlated molecular calculations. VII. Valence, core-valence, and scalar relativistic basis sets for Li, Be, Na, and Mg. *Theor. Chem. Acc.* **2011**, *128*, 69–82.

(32) Papajak, E.; Zheng, J.; Xu, X.; Leverentz, H. R.; Truhlar, D. G. Perspectives on Basis Sets Beautiful: Seasonal Plantings of Diffuse Basis Functions. *J. Chem. Theory Comput.* **2011**, *7*, 3027–3034.

(33) Bartlett, R. J.; Ravi, M.; Park, Y. C.; Bauman, N. P.; Melnichuk, A.; Ranasinghe, D.; Perera, A. Index of multi-determinantal and multi-reference character in coupled-cluster theory. *J. Chem. Phys.* **2020**, *153*, 234103.

(34) Angeli, C.; Cimiraglia, R.; Malrieu, J.-P. *n*-electron valence state perturbation theory:

A spinless formulation and an efficient implementation of the strongly contracted and of the partially contracted variants. *J. Chem. Phys.* **2002**, *117*, 9138–9153.

(35) Mertins, F.; Schirmer, J.; Tarantelli, A. Algebraic Propagotor Approaches and Intermediate-State Representations. II. The Equation-Of-Motion Methods for N, $N\pm1$, and $N \pm 2$ Electrons. *Phys. Rev. A* **1996**, *53*, 2153–2168.

(36) Ehara, M.; Ishida, M.; Toyota, K.; Nakatsuji, H. SAC-CI General-R Method: Theory and Applications to the Multi-Electron Processes. Reviews of Modern Quantum Chemistry. Singapore, 2002; pp 293–319.

(37) Riss, U. V.; Meyer, H.-D. Calculation of Resonance Energies and Widths using the Complex Absorbing Potential Method. *J. Phys. B* **1993**, *26*, 4503–4535.

(38) Sommerfeld, T.; Ehara, M. Complex Absorbing Potentials with Voronoi Isosurfaces Wrapping Perfectly around Molecules. *J. Chem. Theoy. Comput.* **2015**, *11*, 4627–4633.

(39) Ehara, M.; Fukuda, R.; Sommerfeld, T. Projected CAP/SAC-CI Method with Smooth Voronoi Potential for Calculating Resonance States. *J. Comput. Chem.* **2016**, *37*, 242–249.

(40) Andersson, K.; Malmqvist, P. A.; Roos, B. O.; Sadlej, A. J.; Wolinski, K. Second-order perturbation theory with a CASSCF reference function. *J. Phys. Chem.* **1990**, *94*, 5483–5488.

(41) Andersson, K.; Malmqvist, P.-Å.; Roos, B. O. Second-order perturbation theory with a complete active space self-consistent field reference function. *J. Chem. Phys.* **1992**, *96*, 1218–1226.

(42) Shiozaki, T.; Győrffy, W.; Celani, P.; Werner, H.-J. Communication: Extended multi-state complete active space second-order perturbation theory: Energy and nuclear gradients. *J. Chem. Phys.* **2011**, *135*, 081106.

(43) Ghigo, G.; Roos, B. O.; Malmqvist, P.-Å. A modified definition of the zeroth-order Hamiltonian in multiconfigurational perturbation theory (CASPT2). *Chem. Phys. Lett.* **2004**, *396*, 142–149.

(44) Forsberg, N.; Malmqvist, P.-Å. Multiconfiguration perturbation theory with imaginary level shift. *Chem. Phys. Lett.* **1997**, *274*, 196–204.

(45) Sommerfeld, T.; Santra, R. An efficient method to perform CAP/CI calculations for temporary anions. *Int. J. Quant. Chem.* **2001**, *82*, 218.

(46) Frisch, M. J.; Trucks, G. W.; Schlegel, H. B.; Scuseria, G. E.; Robb, M. A.; Cheeseman, J. R.; Scalmani, G.; Barone, V.; Mennucci, B.; Petersson, G. A.; et. al., Gaussian 09 Revision B.01. Gaussian Inc. Wallingford CT 2009.

(47) Matthews, D. A.; Cheng, L.; Harding, M. E.; Lipparini, F.; Stopkowicz, S.; Jagau, T.-C.; Szalay, P. G.; Gauss, J.; Stanton, J. F. Coupled-cluster techniques for computational chemistry: The CFOUR program package. *J. Chem. Phys.* **2020**, *152*, 214108.

(48) Yanai, T.; Kurashige, Y.; Mizukami, W.; Chalupský, J.; Lan, T. N.; Saitow, M. Density Matrix Renormalization Group for Ab Initio Calculations and Associated Dynamic Correlation Methods: A Review of Theory and Applications. *Int. J. Quantum Chem.* **2015**, *115*, 283–299.

(49) Neese, F.; Wennmohs, F.; Becker, U.; Riplinger, C. The ORCA quantum chemistry program package. *J. Chem. Phys.* **2020**, *152*, 224108.

(50) Dutta, A. K.; Neesea, F.; Izsák, R. Towards a pair natural orbital coupled cluster method for excited states. *J. Chem. Phys.* **2016**, *145*, 034102.

(51) Homray, M.; Mondal, S.; Misra, A.; Chattaraj, P. K. Bond stretch isomerism in Be_3^{2-} driven by the Renner-Teller effect. *Phys. Chem. Chem. Phys.* **2019**, *21*, 7996–8003.

(52) Simons, J. Theoretical Study of Negative Molecular Ions. *Ann. Rev. Phys. Chem.* **2011**, *62*, 107–128.

(53) Falcetta, M. F.; Reilly, N. D.; Jordan, K. D. Stabilization calculations of the low-lying temporary anions states of Be, Mg, and Ca. *Chem. Phys. Lett.* **2017**, *482*, 239–243.

(54) Feuerbacher, S.; Sommerfeld, T.; Cederbaum, L. S. Intersection of potential energy surfaces of short-lived states: the complex analogue of conical intersections. *J. Chem. Phys.* **2004**, *120*, 3201.

(55) Weigend, F.; Ahlrichs, R. Balanced basis sets of split valence, triple zeta valence and quadruple zeta valence quality for H to Rn: Design and assessment of accuracy. *Phys. Chem. Chem. Phys.* **2005**, *7*, 3297.

(56) Zheng, J.; Xu, X.; Truhlar, D. G. Minimally augmented Karlsruhe basis sets. *Theo. Chem. Acc.* **2011**, *128*, 295–305.

TOC graphics

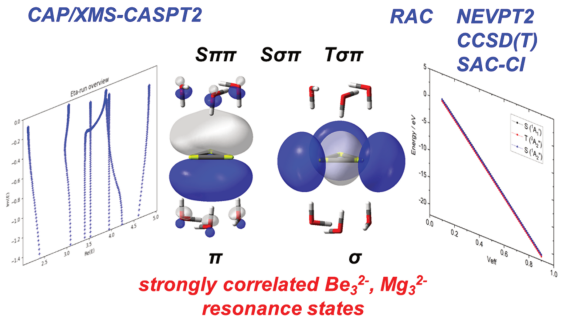

Supporting Information Available

S1 Complex absorbing potentials: η-trajectories

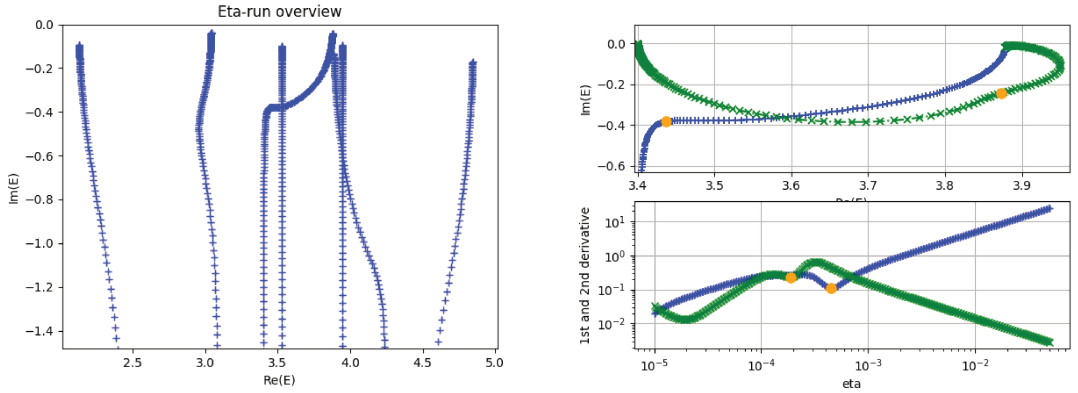

Figure S1: The η-trajectories of the Be_3^{2-} $S_{\pi\pi}$, calculated with CAP/XMS-CASPT2, CAS(7,12)+n_{virt}, $n_{\mathrm{virt}} = 5$, seven roots, R(Be–Be) = 2.15 Å.

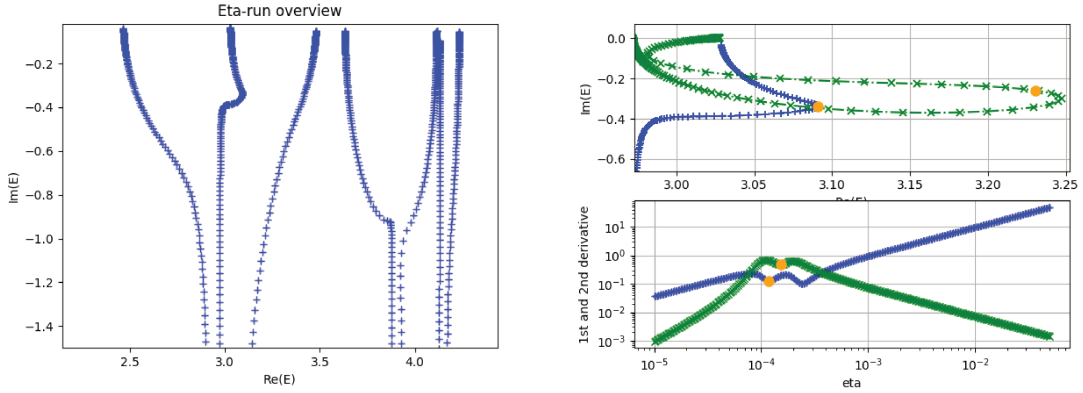

Figure S2: The η-trajectories of the Be_3^{2-} $S_{\sigma\sigma}$, calculated with CAP/XMS-CASPT2, CAS(7,12)+n_{virt}, $n_{\mathrm{virt}} = 4$, seven roots, R(Be–Be) = 2.15 Å.

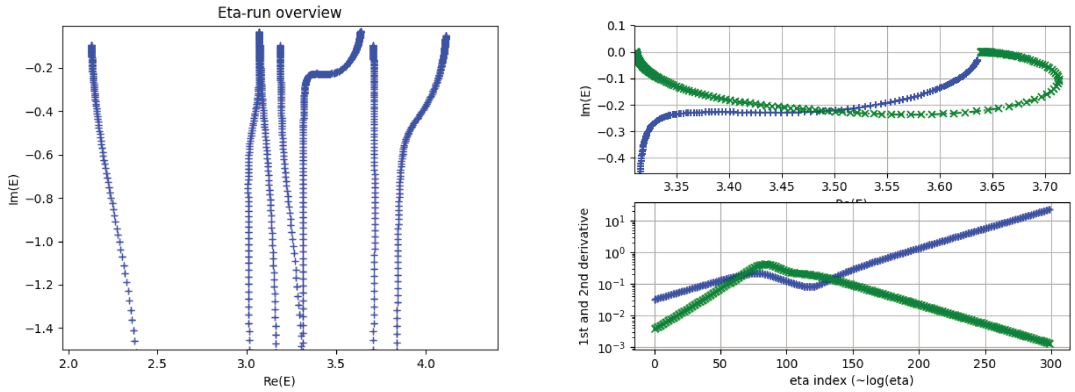

Figure S3: The η-trajectories of the Be_3^{2-} $S_{\sigma\pi}$, calculated with CAP/XMS-CASPT2, CAS(7,12)+n_{virt}, $n_{\mathrm{virt}} = 5$, seven roots, R(Be–Be) = 2.15 Å.

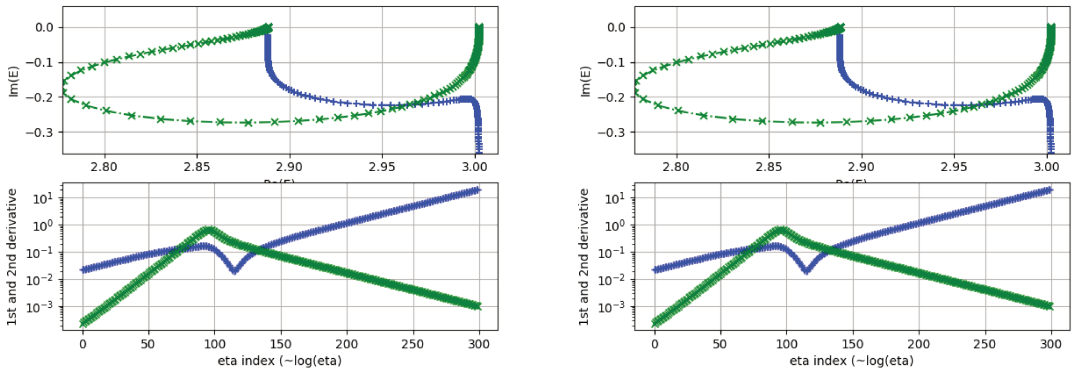

Figure S4: The η-trajectories of the Be_3^{2-} $T_{\sigma\pi}$, calculated with CAP/XMS-CASPT2, CAS(7,12)+n_{virt}, $n_{\mathrm{virt}} = 5$, seven roots, R(Be–Be) = 2.15 Å.

S2 Cartesian coordinates for model solvation

$Be_3((H_2O)_3)_2^{2-}$

Be	-0.001128	-0.000025	1.214306
Be	1.048223	-0.002427	-0.601122
Be	-1.048157	0.003428	-0.601729
O	0.051563	-3.475770	-1.697414
O	-1.512858	-3.469815	0.794340
O	1.424754	-3.475679	0.899962
O	-0.049684	3.476103	-1.697423
O	-1.425268	3.476263	0.898245
O	1.511957	3.468528	0.796203
H	-0.734800	3.609741	-1.015892
H	1.275878	3.598005	-0.141288
H	-0.494028	3.595699	1.163119
H	0.736119	-3.609357	-1.015332
H	0.493274	-3.595708	1.163677
H	-1.275131	-3.598992	-0.142780
H	-1.460002	-2.493353	0.866292
H	-0.033422	-2.499064	-1.686232
H	1.468961	-2.499730	0.815634
H	-1.469942	2.500345	0.813826
H	1.458579	2.492082	0.867963
H	0.035071	2.499368	-1.686142

$\mathbf{Mg_3((H_2O)_3)_2^{2-}}$

Mg	-0.001205	0.000094	1.706632
Mg	1.476520	-0.011426	-0.846913
Mg	-1.475932	0.011718	-0.848637
O	-0.024368	-4.112653	-1.682586
O	-1.483258	-4.105149	0.833566
O	1.423598	-4.134317	0.841000
O	0.026656	4.112692	-1.682205
O	-1.424306	4.134323	0.839597
O	1.482457	4.104640	0.835659
H	-0.692305	4.187303	-1.024859
H	1.275863	4.169930	-0.117060
H	-0.494136	4.197848	1.131915
H	0.693828	-4.187158	-1.024401
H	0.493104	-4.198038	1.132216
H	-1.275460	-4.170330	-0.118891
H	-1.567072	-3.142955	0.961880
H	-0.077795	-3.149960	-1.822729
H	1.582626	-3.173406	0.864377
H	-1.583479	3.173426	0.862683
H	1.565930	3.142405	0.963941
H	0.080039	3.149984	-1.822297

$\mathbf{Be_3((H_2O)_6)_2^{2-}}$

Be	0.001683	-0.000151	1.201369
Be	1.048033	-0.000007	-0.612828
Be	-1.045514	-0.000688	-0.612196
O	1.411487	-3.334470	0.891737
O	0.076891	-3.339334	-1.689819
O	-1.498856	-3.333022	0.760577
O	-1.409968	3.333253	0.891884
O	1.500109	3.334396	0.760049
O	-0.076651	3.339361	-1.690003
O	1.561295	-6.192949	0.660228
O	-1.337664	-6.185048	1.042969
O	-0.221014	-6.197184	-1.659632
O	1.336196	6.186301	1.042692
O	0.218756	6.197571	-1.659595
O	-1.562771	6.191473	0.660951
H	-0.470094	3.336404	1.159047
H	-0.774965	3.351148	-1.006508
H	1.259899	3.350746	-0.186821
H	0.471703	-3.336798	1.159218
H	-1.258936	-3.349533	-0.186362
H	0.775484	-3.351753	-1.006637
H	-0.076640	-2.373470	-1.779635
H	1.574983	-2.369991	0.803474
H	-1.493682	-2.366399	0.935923
H	1.495837	2.367769	0.935409
H	0.077732	2.373655	-1.779964

H	-1.572641	2.368590	0.803834
H	0.378636	6.240761	1.215508
H	0.844046	6.249068	-0.913807
H	-1.232586	6.251311	-0.253982
H	1.230694	-6.252430	-0.254581
H	-0.846134	-6.248189	-0.913670
H	-0.380111	-6.240442	1.215484
H	-0.232123	-5.255691	-1.909432
H	1.773735	-5.248512	0.769714
H	-1.542307	-5.240472	1.165761
H	1.541797	5.241920	1.165358
H	-1.774218	5.246808	0.770461
H	0.230647	5.256110	-1.909478